Quadruped Bounding Control with Variable Duty Cycle via Vertical Impulse Scaling

Quadruped Bounding Control with Variable Duty Cycle via Vertical Impulse Scaling

Hae-Won Park[1], Meng Yee (Michael) Chuah[1], and Sangbae Kim[1]

***Abstract*— This paper introduces a bounding gait control algorithm that allows a successful implementation of duty cycle modulation in the MIT Cheetah 2. Instead of controlling leg stiffness to emulate a 'springy leg' inspired from the Spring-Loaded-Inverted-Pendulum (SLIP) model, the algorithm prescribes vertical impulse by generating scaled ground reaction forces at each step to achieve the desired stance and total stride duration. Therefore, we can control the duty cycle: the percentage of the stance phase over the entire cycle. By prescribing the required vertical impulse of the ground reaction force at each step, the algorithm can adapt to variable duty cycles attributed to variations in running speed. Following linear momentum conservation law, in order to achieve a limit-cycle gait, the sum of all vertical ground reaction forces must match vertical momentum created by gravity during a cycle. In addition, we added a virtual compliance control in the vertical direction to enhance stability. The stiffness of the virtual compliance is selected based on the eigenvalue analysis of the linearized Poincaré map and the chosen stiffness is 700 N/m, which corresponds to around 12% of the stiffness used in the previous trotting experiments of the MIT Cheetah, where the ground reaction forces are purely caused by the impedance controller with equilibrium point trajectories. This indicates that the virtual compliance control does not significantly contributes to generating ground reaction forces, but to stability. The experimental results show that the algorithm successfully prescribes the duty cycle for stable bounding gaits. This new approach can shed a light on variable speed running control algorithm.**

I. INTRODUCTION

Recent advances in quadrupedal robots show a remarkable performance. Several robots developed by Boston Dynamics began to unveil the potential advantage of four-legged morphology by demonstrating robust gait control [1], and fast locomotion [2]. While these robots take advantage of a high energy density source - gasoline, the MIT Cheetah 2 employs a unique electric actuation system and achieved a fast (13.5 mph) and high energy efficiency (Total cost of transport: 0.51) running rivaling animals in a similar scale [3]. StarlETH [4] and HyQ [5] also demonstrate an impressive robustness on rough terrain walking. These advancements show that robotic quadrupdalism has a great potential to be a future transportation mode.

In developing legged robots, biomechanical studies on animals have significantly influenced the engineering endeavor to design controllers for quadrupedal locomotion. Biologists suggested a simple model, the Spring-Loaded-Inverted-Pendulum (SLIP) that well represents the center of mass behaviors of steady state symmetric running gaits [6], [7]. The introduction of the SLIP model spawned a number of studies on legged running. Study in [8] focused on comparing various kinds of gaits using the SLIP model. Nanua [9] developed a simple control strategy for the galloping gait based on Raibert's controller [10] and analyzed the stability of the gait in a simulation model. Also, studies on quadrupedal gait controllers use passive compliance model at each leg similar to the SLIP model [11], [12], [13].

The introduction of SLIP model has significantly influenced the hardware design of quadrupedal robots. Poulakakis [14] suggested the utilization of the natural stability of the system with passive compliances in the legs, the physical embodiment of which became mechanical springs at the prismatic legs in Scout II. Cheetah-cub also employs physical springs to achieve stable, dynamic running [15]. Haynes [16] utilizes passive compliance of curved composite leg design with a passive spine. StarlETH [4] employs a series elastic actuator at each leg to achieve a dynamic walking gait. Although many robots demonstrate successful locomotion, still most of them stay in a slow speed range ($< Fr = 1.3$) and it is not clear how to optimize the leg impedance for maximum stability in a wide range of speed.

In contrast to the effort to emulate the 'springy leg', a few recent studies investigated the direct control of ground reaction forces. Koepl modeled a spring-mass system with a force-controlled actuator and the algorithm commands forces according to an ideal model of the passive dynamics [17]. The study shows the potential advantages of a ground force tracking approach over a passive spring leg approach in ground disturbance rejection. Valenzuela introduces an algorithm that uses optimum forces and torques acting on the hip, focusing on the body dynamics with an assumption that the leg mass and inertia are significantly smaller than those of the body [18]. However, successful implementation of ground reaction force control for running robots has been a difficult challenge due to the high bandwidth requirement and contact instability caused by non-collocated force sensing feedback [19].

Utilizing a unique high bandwidth actuation of the MIT Cheetah 2, we aim to control the stance time and aerial time by scaling ground reaction forces to achieve variable speed running. The duty cycle naturally drops as running speed increases because the stance time is limited by the stroke length divided by the forward running speed. The experimental data of dog running show that the stance

This work was supported by the Defense Advanced Research Program Agency M3 program

[1]Authors are with the Department of Mechanical Engineering, Massachusetts Institute of Technology, Cambridge, MA, 02139, USA , corresponding email: parkhw at mit.edu

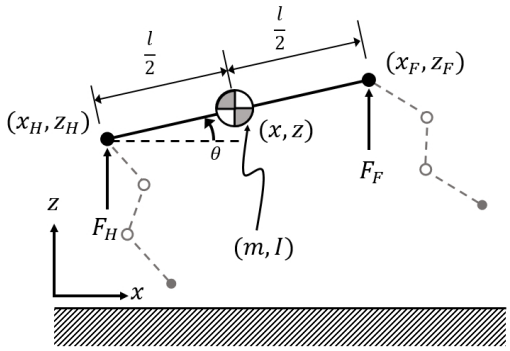

Fig. 1. Simplified Sagittal Plane Model of the MIT Cheetah 2 Robot. The legs are modeled as massless, and the effect of the legs on the body's dynamics are included as forces at the shoulder of the robot similar to [18].

time decreases as the running speed increases, whereas the swing time remains constant over a wide range of speeds [20]. Therefore, the duty cycle decreases as the running speed increases. In order to achieve a periodic running gait, according to linear momentum conservation law, the sum of all ground reaction forces must match vertical momentum loss due to gravity during a cycle. This means quadrupeds should be able to scale the ground reaction force according to decrease in stance time attributed to the running speed.

In this paper, we introduce a new algorithm that allows accurate prescription of the stance duration in a bounding gait of the MIT Cheetah 2. Instead of controlling leg stiffness and the equilibrium point trajectories, the leg control algorithm tracks a prescribed ground reaction force profile determined by the desired stance duration and swing phase duration. This technique allows modulation of the duty cycle of bounding, taking advantage of the high bandwidth and low inertia leg of the MIT Cheetah 2.

The remainder of the paper is organized as follows: Section II explains the underlying principles of the vertical impulse control algorithm that allows duty cycle modulation. Section III details how the controller is implemented. Section IV summarize the experimental results of bounding gait of the MIT Cheetah 2. Section V concludes the paper and discusses future research direction.

II. Duty Cycle Modulation via Scaling of Vertical Impulse

This section presents the concepts of duty cycle modulation via scaling vertical impulse in the context of a simple two-legged model that represents a quadruped in the sagittal plane. Given that the relative distance the robot contacts with the ground during the stance is limited by the workspace of the leg, the stance duration should be decreased as the running speed increases. In this paper, among the various running gaits of quadrupeds, only the bounding gait is studied for the sake of brevity. The duty cycle of bounding is modulated via changing the duration of stance while keeping the duration of swing constant.

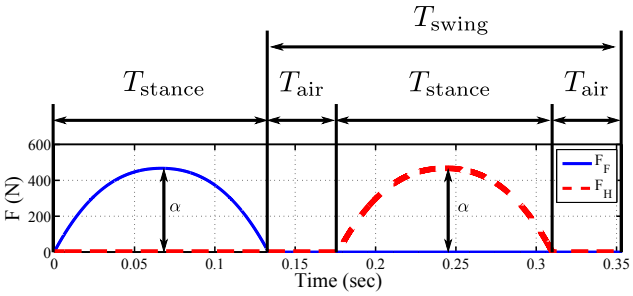

Fig. 2. Force profile when $T_{\text{stance}} = 133$ msec and $T_{\text{swing}} = 220$ msec.

A. Simplified Sagittal Plane Model

A quadruped runner can be modeled as a two-legged sagittal plane model, as shown in Figure 1, because we restrict our attention to the bounding gait where front and hind pairs of the leg act as in parallel [21]. The generalized coordinates of the robot are taken as $q := (x, z, \theta)$. This model assumes massless legs and the effect of the leg on the body's dynamics is represented by the vertical direction forces F_F and F_H at the front and hind shoulder of the body. The equations of motion of the body are shown below.

$$\begin{aligned} \ddot{x} &= 0 \\ \ddot{z} &= -g + \frac{F_F}{m} + \frac{F_H}{m} \\ \ddot{\theta} &= F_F \frac{l}{2I}\cos\theta - F_H \frac{l}{2I}\cos\theta \end{aligned} \tag{1}$$

The body's mass m and inertia I are 31 kg and 2.9 kgm^2 respectively, length l of the body is 0.7 m, and the center of mass is located in the middle of the body. All the inertial and kinematic parameters are drawn from the MIT Cheetah 2 robot.

The model is symmetric in the fore-aft direction, and dynamics in the direction of x and z are decoupled from each other. Therefore, we can assume the control of the vertical and horizontal direction as separate problems. This can be clearly seen from the equation of motions above. In particular, horizontal speed control becomes trivial in this model because the horizontal momentum $m\dot{x}$ will be conserved as specified by an initial condition unless there are external forces in the direction of x. Hence, we only focus on the control of vertical motion during bounding in this paper.

B. Selection of Force Profile

The force profile $F_i,\ \mathrm{i} \in \mathrm{F}, \mathrm{H}$, which represents the effect of the leg on the body's dynamics, is chosen such as to provide periodic limit cycle bounding with the desired duty cycle. Here, the subscripts F and H represent the front and hind legs, respectively. Time-dependent force profile for F_i shown in Figure 2 is parametrized as,

$$F_i = h(\alpha, t, T_{\text{stance}}, T_{\text{swing}}),\ \text{for}\ i = F, H, \tag{2}$$

where α is the scalar value representing the magnitude of the force profile, as depicted in Figure 2, t is the time counted from the beginning of the step, T_{stance} is the duration of the stance where the legs affects the dynamics of the body by the forces at the shoulder, and T_{swing} is the duration of the swing where the leg is not touching the ground. The force profile of the front leg is made up of 3$^{\text{rd}}$-order Bézier polynomials, where the Bézier coefficients are given by,

$$\beta = \begin{cases} \alpha\,[0.0\ 0.8\ 1.0\ 1.0] & 0 < t < \frac{1}{2}T_{\text{stance}} \\ \alpha\,[1.0\ 1.0\ 0.8\ 0.0] & \frac{1}{2}T_{\text{stance}} < t < T_{\text{stance}} \\ [0.0\ 0.0\ 0.0\ 0.0] & \text{otherwise} \end{cases} \tag{3}$$

These coefficients are chosen to ensure smooth continuity between the first two Bézier polynomials, and for easy scaling of the force profile. The Bézier coefficients for force profile of the hind leg are identical.

The two airborne durations in the middle of the stride and at the end of the stride where both legs are not touching the ground are assumed to be equal for the sake of simplicity, and hence calculated as,

$$T_{air} = \frac{T_{\text{swing}} - T_{\text{stance}}}{2} \tag{4}$$

Additional simplification can be done by assuming the same scalar value α for the front and hind legs. Furthermore, without loss of generality, we can suppose that the step always starts with the force profile for the front leg, followed by the first airborne duration, and second force profile for the hind leg, and ends with second airborne duration, as illustrated in Figure 2. Duration of the swing phase T_{swing} can be chosen as any value. However, the choice of T_{swing} provides a chance to make use of insights from biology. In the case of a quadrupedal robot, insights can be drawn from steady running locomotion of cheetahs and dogs. Several bio-mechanical studies of animal galloping found that swing duration remains relatively constant within a range of 0.22-0.3 sec over a wide range of locomotion speeds [20], or had a weak trend with speed [22]. Drawing from this biological observation, further simplification can be done by keeping the duration of the swing phase T_{swing} a constant value at 0.22 sec for a wide range of T_{stance}. The lowest value of T_{swing} was chosen so as to keep the vertical height of the robot manageable during the aerial phase.

C. Modulation of Stance Duration

From the Sections II-A and II-B, we can see that only two remaining parameters remain undefined for describing the force profile, which are the duration of stance T_{stance} and the magnitude of the force profile α. Here, we will draw the relation between those two parameters, using the principle that the total vertical impulse during one period of cyclic locomotion must be equal to the total gravitational impulse to satisfy momentum conservation in steady state running. This is described in the following equation,

$$\sum^{i} \int_0^T F_i dt = mgT \tag{5}$$

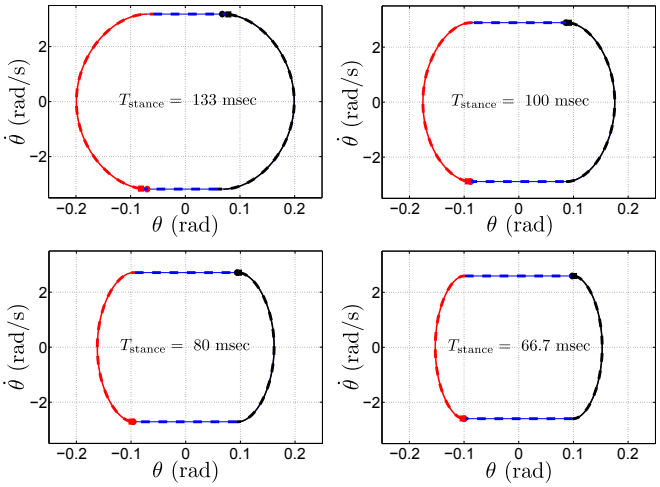

Fig. 3. Phase plot of body pitch angle θ for periodic limit cycle of open-loop system (solid line) and closed-loop system (dashed-line). Red line represents the front leg stance phase, and start of the stance phase is represented by the square or circle respectively. Black line represents the hind leg stance phase, and start of the stance phase is represented by the square or circle respectively. Blue line represents the airborne durations. Top Left: $T_{\text{stance}} = 133$ msec ($D = 0.377$) Top Right: $T_{\text{stance}} = 100$ msec ($D = 0.312$) Bottom Right: $T_{\text{stance}} = 80$ msec ($D = 0.267$) Bottom Right: $T_{\text{stance}} = 66.7$ msec ($D = 0.233$)

where $T := T_{\text{stance}} + T_{\text{swing}}$ is the total duration of one step. Using the assumption that the two force profiles for the front and hind legs are identical, the equation is further simplified into,

$$2\int_0^T F dt = mgT \tag{6}$$

Because the area under the Bézier curve can be simply calculated by averaging the Bézier coefficients multiplied by the length of duration, (6) is rewritten by,

$$2\alpha c T_{stance} = mgT, \tag{7}$$

where $c = \text{E}\left[\frac{1}{2}[0.0\ 0.8\ 1.0\ 1.0] + \frac{1}{2}[1.0\ 1.0\ 0.8\ 0.0]\right]$ is the unit area under the force profile when $\alpha = 1$ and $T_{\text{stance}} = 1$. From (7), α is given by,

$$\alpha = \frac{mgT}{2cT_{\text{stance}}} \tag{8}$$

Equation 8 will be used to calculate the magnitude of force profile α when T_{stance} is given. Now, all the parameters associated with force profile are defined given the value of T_{stance}. Figure 2 shows an example of force profile when $T_{\text{stance}} = 0.133$ sec. In the next section, we will search for periodic limit cycles using various values of T_{stance} .

D. Periodic Limit Cycle

Periodic limit cycles have been found by searching for fixed points of the following Poincaré return map, as defined by $\mathcal{P} : \{(x,t)\,|t = 0\} \rightarrow \{(x,t)\,|t = T\}$[1],

$$x^* = \mathcal{P}(x^*, T_{\text{stance}}), \tag{9}$$

[1]Application of time-dependent force profile causes non-autonomous dynamic system, resulting in Poincaré section with states x and time t [23].

A large number of fixed points have been computed for $T_{\text{stance}} \in [0.0615\ 0.133]$ sec (corresponds to duty cycle $D \in [0.219\ 0.377]$) numerically using MATLAB's `fmincon` function. Figure 3 shows the obtained periodic limit cycle for $T_{\text{stance}} = 133, 100, 80, 66.7$ msec ($D = 0.377, 0.312, 0.267, 0.233$) represented by solid line. Linearizing (9) about the fixed point x^* corresponding to the periodic orbit results in a discrete linear system, which is given by,

$$\Delta x[i+1] = A\Delta x[i], \tag{10}$$

where $\Delta x = x - x^*$, and

$$A = \left.\frac{\partial \mathcal{P}}{\partial x}\right|_{x=x^*}. \tag{11}$$

Calculation of the largest eigenvalue of matrices A corresponding to the $T_{\text{stance}} \in [0.0615\ 0.133]$ sec revealed that the obtained periodic limit cycles are unstable.

E. Feedback Control

In order to obtain locally stabilized periodic limit cycles, we introduce a simple feedback controller during the stance phase. Hence, following simple PD control is added onto force profile F_i as seen in (2),

$$F_{fb} = -k_{p,z}(z_i - z_d) - k_{d,z}(\dot{z}_i), \text{ for } i = \text{F}, \text{H}, \tag{12}$$

where, $k_{p,z}$ is the stiffness, $k_{d,z}$ is the damping, z_d, is the set point value which is constant throughout the stance phase and selected as the averaged value of $z_{\text{F,H}}$ of the open-loop periodic orbit during the stance phase. We could use time-dependent trajectory for $z_d(t)$ obtained from the corresponding periodic limit cycle to exactly track the open-loop trajectory, but this causes different sets of trajectories $z_d(t)$ for different values of T_{stance}. Because our focus is to obtain a stable periodic limit cycle for various T_{stance} rather than to follow exact trajectories, a single set point value for all the case of T_{stance} is sought for in this paper. Damping $k_{d,z}$ is chosen as 30 Ns/m for the simulation which is the maximum value until the real-hardware becomes unstable due to the noise caused from the numerical differentiation of the encoder signal.

Because feedback is added onto the original force profile and influences the dynamics of the system, the behavior of the system will be changed accordingly. Therefore, new fixed points should be calculated numerically. A large number of fixed points have been computed for different values of $T_{\text{stance}} \in [0.0615\ 0.133]$ sec and $k \in [0, 3000]$.

$$\bar{x}^* = \mathcal{P}(\bar{x}^*, k_{p,z}, T_{\text{stance}}). \tag{13}$$

The eigenvalues of linearized Poincaré map A for $k_{p,z} \in [0, 3000]$ and $T_{\text{stance}} \in [0.0615, 0.133]$ are calculated, and the largest eigenvalues are plotted in Figure 4. The result shows that addition of the feedback yields stable periodic orbit for a wide range of the value of $k_{p,z}$ for all $T_{\text{stance}} \in [0.0615, 0.133]$. The stable region is depicted by the area enclosed by the solid red line, and $k_{p,z}$ is selected as 700 N/m because the value provides stable periodic limit cycle for all $T_{\text{stance}} \in [0.0615, 0.133]$. We would like note that this value of stiffness 700 N/m is around 12% of the stiffness value used in the previous trotting experiments of MIT Cheetah where only a impedance controller is used.

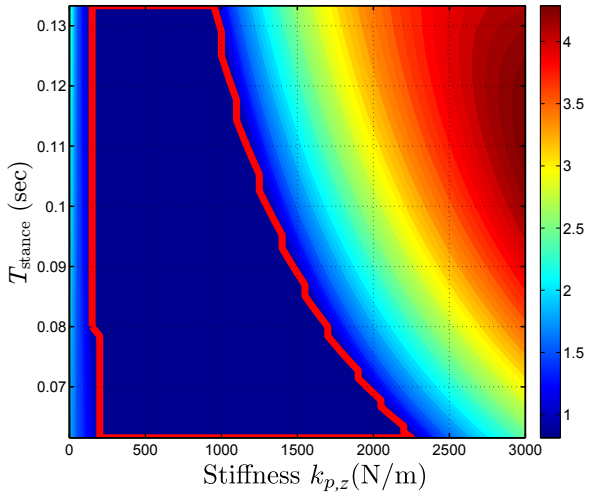

Fig. 4. The largest eigenvalues of linearized Poincaré map for $k_{p,z} \in [0, 3000]$ and $T_{\text{stance}} \in [0.0615, 0.133]$. The area enclosed by solid red line represents the largest eigenvalue is less than 1 which means locally exponentially stable about the fixed point $\bar{x}^*$.

Dashed lines of Figure 3 show the phase plot of body pitch angle θ for closed-loop system. Addition of feedback could successfully stabilizes the open-loop system's periodic orbits without changing them.

III. Implementation of the Algorithm

This section presents the implementation of the algorithm introduced in Section II on the real robot hardware. Only vertical motion is considered in this paper, and force profiles F_i, where $i = F, H$, obtained from Section II will be implemented in the robot through the torques of the two coaxial motors in the MIT Cheetah 2 as shown in Figure 5. Each leg of the MIT Cheetah 2 consists of three links, and the motions of first and last link from the shoulder are kinematically tied to be parallel to each other as shown in Figure 5(a), resulting in two degree of freedom links. The first actuator rotates the link represented by thick solid black line, providing rotation of all three links relative to the body. The second actuator rotates the link represented by dashed red line, yielding rotation of second link while first and third links are kept in parallel. Because the first and third links are parallel, the original link structure can be kinematically converted to a mechanism with only two links shown in Figure 5(b).

A. Application of Force Profile and Feedback

The algorithm we obtained in Section II of combining force profile and feedback with low gain is implemented on the robot using actuator torques on the leg. We could calculate the exact required actuator torques to provide desired horizontal and vertical direction ground reaction force from solving inverse dynamics, but the following static

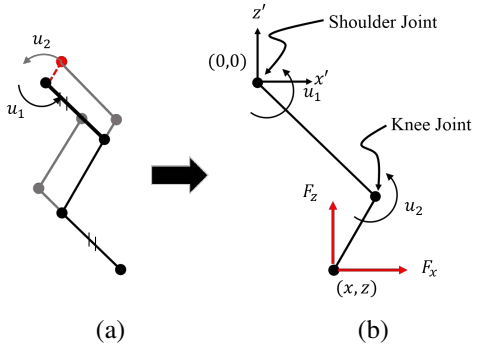

Fig. 5. (a) MIT Cheetah's leg consisting of three links. First and third links are kept in parallel each other by parallelogram mechanism. (b) Two links kinematic conversion of original link structure. Body coordinates system x'-z' is attached on the shoulder.

force/torque relationship is only considered in this paper instead.

$$u = J_{xz}^T \begin{bmatrix} F_x \\ F_z \end{bmatrix} \tag{14}$$

where x and z are the horizontal and vertical position of the foot relative to the shoulder respectively as shown in Figure 5, F_x and F_y are desired ground reaction forces in x and z direction, and J_{xz} is the manipulator Jacobian obtained by taking partial derivative of position of the foot relative to the shoulder with respect to the knee and shoulder joint angles. This approximation of the calculating control inputs is reasonable because the robots leg is relatively light compared to the body (less than 10% of body mass). Furthermore, it removes all the complex calculation of the Coriolis matrix and the inverse of the inertia matrix, making implementation simpler and easier with regular joint encoders and signals from an IMU sensor. A similar approach introduced in [24] which also only takes static force/torque relationships have been successfully implemented and tested experimentally on their robot with extremely light legs [24], [25].

To hold the horizontal position of the foot in place, the horizontal direction force F_x is chosen as,

$$F_x = -k_{p,x}x - k_{d,x}\dot{x} \tag{15}$$

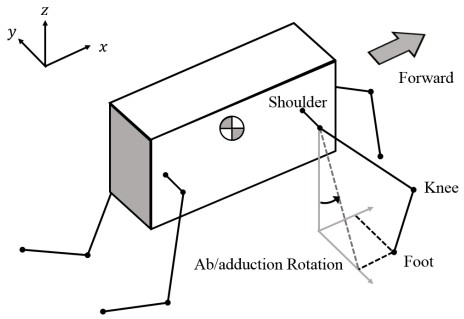

Fig. 6. Coordinates system for control of MIT Cheetah 2. In addition to actuators for knee and shoulder angles, there is one more actuator for ab/adduction rotation for each leg.

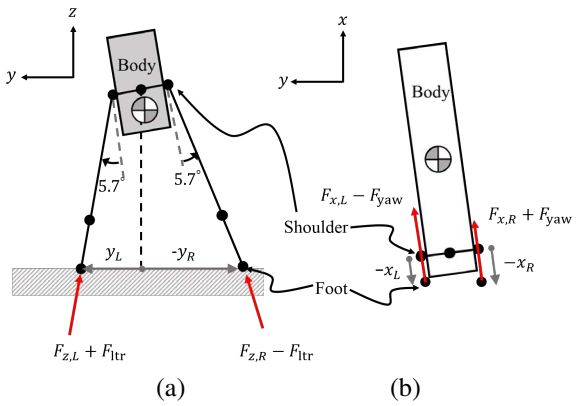

Fig. 7. Lateral and yaw motion control. (a) Lateral motion is regulated using z-direction forces on the both feet. (b) Yaw is regulated using x-direction forces on the both feet.

The vertical direction force F_z is chosen as,

$$F_z = F_i - k_{p,z}(z - z_d) - k_{d,z}\dot{z}, \text{ for } i = F, H \tag{16}$$

where F_i is predefined force profile as in (2) and (3) corresponding to the desired T_{stance}. The scalar gain value $k_{p,x}$ and $k_{d,x}$ is the stiffness and damping for PD control in the x direction which are chosen as $2100\ \text{N/m}$ and $14\ \text{Ns/m}$ and $k_{p,z}$ and $k_{d,z}$ is the stiffness and damping for PD control in the z direction which are chosen as $700\ \text{N/m}$ and $30\ \text{Ns/m}$ as in Section II, and z_d is the set point for PD control, selected as $-0.5\ \text{m}$

B. Lateral and Yaw Motion Control

Because the robot can freely move in 3D without any support mechanism, we have to regulate yaw and lateral motion of the robot. Figure 6 depicts the coordinates system for yaw and lateral motion control of MIT Cheetah 2 and actuators for ab/adduction rotation. Here, the motor for controlling ab/adduction rotation of the leg is commanded to hold 5.7 degrees outward as shown in Figure 7(a) to provide postural lateral stability[2]. However, lateral instability is still observed due to the small difference of the motor characteristics and leg kinematics between left and right legs. Therefore, feedback is added to stabilize lateral motion. During the double support phase of the left and right leg, as shown in Figure 7(a), the control authority on lateral motion obtained from the difference between $F_{z,L}$ and $F_{z,R}$ is used to regulate lateral motion. The objective of the feedback is to drive following error to zero,

$$e_{\text{ltr}} = y_L + y_R, \tag{17}$$

where, the subscripts L and R indicate the left and right legs, respectively. The following feedback given by,

$$F_{\text{ltr}} = -K_{p,\text{ltr}}e_{\text{ltr}} - K_{d,\text{ltr}}\dot{e}_{\text{ltr}} \tag{18}$$

[2]The motor used for ab/adduction is off-the-shelf servo motor which is designed for precise position control and not for force control. Hence, it is not used for lateral and yaw motion control.

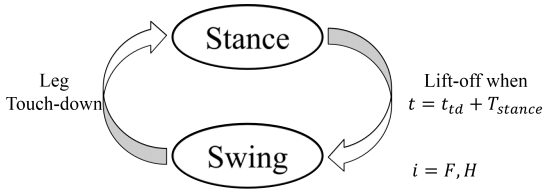

Fig. 8. Stance Machine for front and hind legs.

is added onto vertical direction force F_z in (16) as follows,

$$\begin{aligned} F_{z,L} &= F_{z,L} + F_{\mathrm{ltr}} \\ F_{z,R} &= F_{z,R} - F_{\mathrm{ltr}} \end{aligned} \tag{19}$$

By addition of this feedback, when $e_{\mathrm{ltr}} < 0$, that is to say, the mid point of the body is left-sided as shown in Figure 7(a), the positive force F_{ltr} is added onto $F_{z,L}$ and subtracted from $F_{z,R}$, resulting in the motion of the mid point of the body to the right, and vice versa.

The gains for lateral motion control are selected as the largest values before the system goes unstable due to the gain values becoming too large,

$$K_{p,\mathrm{ltr}} = 1200, \;\; K_{d,\mathrm{ltr}} = 20. \tag{20}$$

Rotation about the yaw axis is controlled using the difference between horizontal left and right forces $F_{x,L}$ and $F_{x,R}$ as illustrated in Figure 7(b). The error to be regulated is defined as $e_{\mathrm{yaw}} := x_L - x_R$. The feedback to drive the error e_{yaw} to zero is given by $F_{\mathrm{yaw}} := -K_{p,\mathrm{yaw}} e_{\mathrm{yaw}} - K_{d,\mathrm{yaw}} \dot{e}_{\mathrm{yaw}}$, and added onto the horizontal direction force F_{x} in (15) as follows,

$$\begin{aligned} F_{x,L} &= F_{x,L} - F_{\mathrm{yaw}} \\ F_{x,R} &= F_{x,R} + F_{\mathrm{yaw}}. \end{aligned} \tag{21}$$

The values of gain for yaw control are chosen as the largest values until the system goes unstable due to too large gain values,

$$K_{p,\mathrm{yaw}} = 1000, \;\; K_{d,\mathrm{yaw}} = 10. \tag{22}$$

As horizontal motion of the robot is not restricted, some slight drift is observed in the position of the robot during bounding.

C. Swing Phase Control and Detection of Impact with the Ground

During swing phase, the vertical length of the leg is shortened at the beginning of the swing phase to clear the foot from the ground. The leg then returns to its original length of 0.5 m to prepare the landing. In order to achieve this desired vertical motion of the leg, trajectories of the foot in z direction is designed, and a simple feedback control based on Cartesian-computed torque controller [26] is used to track the designed trajectories. Position x direction is held to zero using feedback.

Impact with the ground is detected by proprioception, observing the force in z direction created by joint actuators.

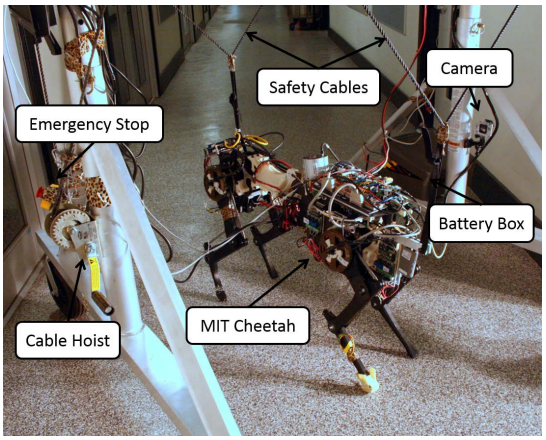

Fig. 9. Experimental setup of the MIT Cheetah 2 robot.

Required nominal z direction force to create the desired swing motion is logged from prior swing leg motion experiments while the robot is hanging in the air. This is used to create a table of nominal forces to reduce incidents of false positives. In the bounding experiment, if z direction force during swing phase is larger than this logged nominal force by some margin, this additional force is assumed to be caused from the impact with the ground and touchdown is declared. However, this could lead to delay in the detection of ground impact during bounding.

D. Finite State Machine

The last step of the implementation process is to introduce a state machine to manage the transition between stance and swing phase for each leg. Two independent finite state machines for each pair of front and hind legs is proposed while transition of a pair of left and right legs occurs together. No synchronization was found to be necessary and there is only an initial phase offset of $T_{\mathrm{stance}} + T_{\mathrm{air}}$ as shown in Figure 2. The state machine is illustrated in Figure 8. Transition from swing to stance occurs when the leg strikes the ground. Transition from stance to swing takes place when time reaches at $T_{\mathrm{stance}} + t_{td}$ where t_{td} is the touchdown time when the leg strikes the ground.

IV. Experiments

This section documents the experimental implementations of the controller introduced in Sections II and III. Figure 9 depicts the experimental setup. The robot stood on four legs until an operator initiates bounding. At the first step, the time-dependent force profile depicted in Figure 2 is applied, and once stance phase of the first step is finished (the legs are airborne), the finite state machine for each pair of legs starts. Experiments were carried out with desired duty ratios $D \in \{0.377, 0.342, 0.312, 0.288, 0.267, 0.248, 0.233, 0.219\}$. In Table I, the experimentally achieved duty cycles and the percentage errors can be seen. The achieved duty cycles were averaged over 10 steps.

The results of the experiments are presented in Figure 10-13. Figure 10 depicts snapshots at 100 msec intervals of

Fig. 10. Snapshots of bounding with duty ratio of 0.36 ($T_{\text{stance}} = 80$ msec and $T_{\text{swing}} = 220$ msec) at intervals of 100 msec. The snapshots progress temporally from top to bottom, and then left to right.

TABLE I
EXPERIMENTALLY ACHIEVED DUTY CYCLES

Desired Duty Cycle	Achieved Duty Cycle	Percentage Error
0.3774	0.3785	0.3068
0.3419	0.3416	0.0894
0.3125	0.3118	0.2279
0.2878	0.2794	2.9188
0.2667	0.2567	3.7388
0.2484	0.2392	3.7395
0.2326	0.2224	4.3493
0.2186	0.2134	2.3804

bounding with duty ratio of 0.267 ($T_{\text{stance}} = 80$ msec and $T_{\text{swing}} = 220$ msec). The phase sequence depicted in Figure 11 shows that desired duty ratios 0.377 (on the top) and 0.219 (on the bottom) with $T_{\text{stance}} = 133$ msec, 61.5 msec and $T_{\text{swing}} = 220$ msec are achieved experimentally.

Figure 12 depicts the vertical force applied at the front (white region) and hind right (grey region) leg with duty ratios $D = 0.377$ (on the top) and $D = 0.219$ (on the bottom). It is observed that feedback (solid black line) is significantly smaller than the predefined force profile (solid blue line), showing that the predefined force profile plays a major role in providing the bounding gait with the desired duty ratio. Figure 13 compares the phase plot of body pitch angle from the simulation and experimental data. Four cases of duty ratio $D \in \{0.3770.3120.2670.233\}$ are compared. There is a noticeable offset between the experimental and simulation data for each plot. This is due to the simulation model assuming that the center of mass is located in the middle of the body while the actual robot's center of mass

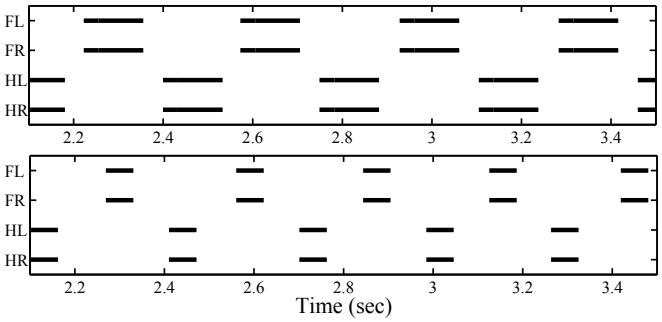

Fig. 11. Phase sequence of the experiments with $T_{\text{stance}} = 133$ msec (on the top) and $T_{\text{stance}} = 61.5$ msec (on the bottom). Black solid line represents stance phase and the empty space represents swing phase. From top to bottom, phase sequences for front left leg (FL), front right leg (FR), hind left leg (HL), hind right leg (HR) are shown.

is located slightly forward (2.3 cm forward from the center). This asymmetry in the position of center of mass causes the robot to tend to tip forward, leading to an offset in pitch. Ripples in the experimental data are caused by cogging torque in the actuators. Another discrepancy occurs when the front leg strikes the ground (see left bottom part of each phase plot). This could be due to the erroneous measurements caused by flexing of the structure holding IMU sensor during ground impact.

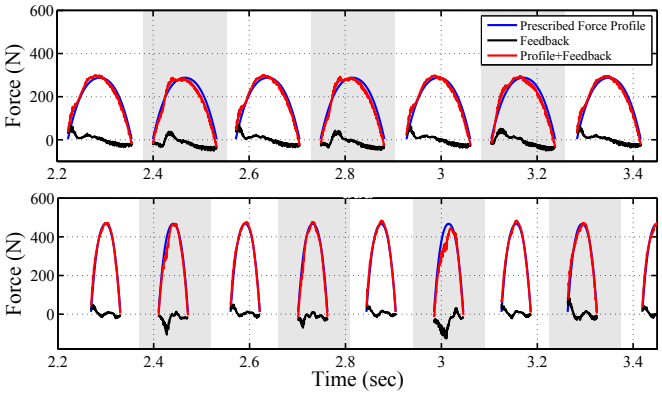

Fig. 12. Vertical Forces applied at the right foot due to force profile, feedback, and a combination of both. White and grey region indicate vertical forces at the front legs and hind legs, respectively. (a) $T_{\text{stance}} = 133$ msec. (b) $T_{\text{stance}} = 61.5$ msec.

V. CONCLUSIONS

We have successfully demonstrated stable quadruped bounding gaits with various duty cycles. A prescribed vertical force profile is combined with a low gain PD control on the height of shoulders, providing stable quadruped bounding in simulation. Next, scaling of vertical impulse based on the principles of vertical momentum balance yields multiple periodic limit cycles with a wide selection of desired duty cycles. The proposed controller has been successfully validated in experiments on the MIT Cheetah 2, achieving stable bounding at different desired duty cycles with regulation of yaw and lateral motion. Currently, this controller is extended to forward running by adding a simple forward speed control.

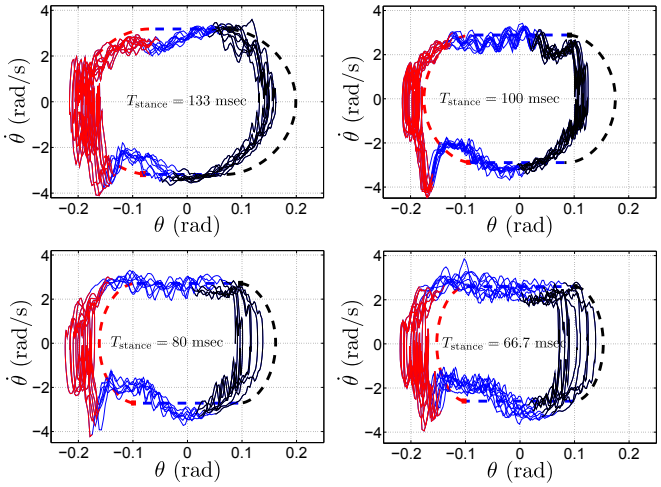

Fig. 13. Phase plot of body pitch angle θ data from the experiments (solid line) and from the simulation (dashed-line). Red line represents front leg stance phase. Black line represents hind leg stance phase. Top Left: $T_{\text{stance}} = 133$ msec ($D = 0.377$) Top Right: $T_{\text{stance}} = 100$ msec ($D = 0.312$) Bottom Right: $T_{\text{stance}} = 80$ msec ($D = 0.267$) Bottom Right: $T_{\text{stance}} = 66.7$ msec ($D = 0.233$)

Preliminary experimental result of bounding with a forward speed of 2 m/sec is shown in Figure 14.

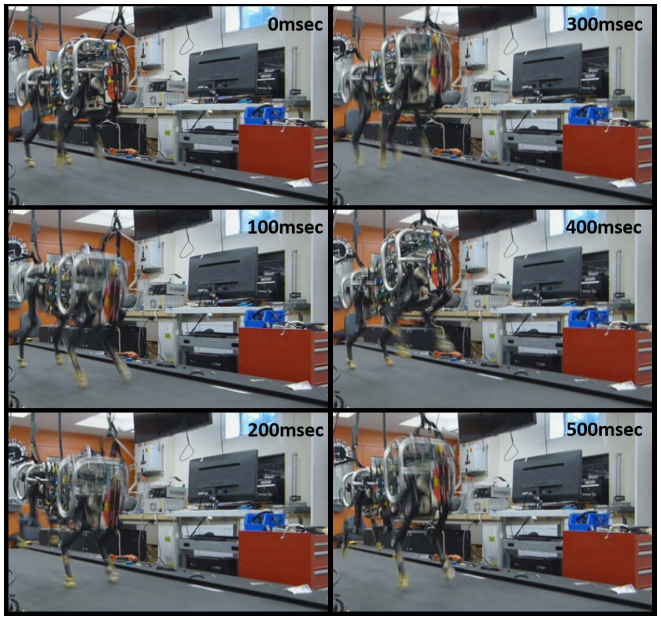

Fig. 14. Preliminary forward running experiment using the proposed controller.

REFERENCES

[1] M. Raibert, K. Blankespoor, G. Nelson, R. Playter, and the BigDog Team, "Bigdog, the rough-terrain quadruped robot," in *Proceedings of the 17th World Congress*, 2008, pp. 10 823–10 825.

[2] Boston Dynamics. (2012) Cheetah robot runs 28.3 mph; a bit faster than usain bolt. Youtube Video. [Online]. Available: http://youtu.be/chPanW0QWhA

[3] D. J. Hyun, S. Seok, J. Lee, and S. Kim, "High speed trot-running: Implementation of a hierarchical controller using proprioceptive impedance control on the MIT cheetah," 2014, manuscript submitted to the International Journal of Robotics Research for publication.

[4] C. Gehring, S. Coros, M. Hutter, M. Bloesch, M. Hoepflinger, and R. Siegwart, "Control of dynamic gaits for a quadrupedal robot," in *Robotics and Automation (ICRA), 2013 IEEE International Conference on*, May 2013, pp. 3287–3292.

[5] C. Semini, N. G. Tsagarakis, E. Guglielmino, M. Focchi, F. Cannella, and D. G. Caldwell, "Design of HyQ: a hydraulically and electrically actuated quadruped robot," *Proceedings of the Institution of Mechanical Engineers, Part I: Journal of Systems and Control Engineering*, vol. 225, no. 6, pp. 831–849, 2011.

[6] R. Blickhan, "The spring-mass model for running and hopping," *Journal of Biomechanics*, vol. 22.

[7] G. A. Cavagna, "Elastic bounce of the body." *Journal of Applied Physiology*, vol. 29, no. 3, pp. 279–82, 1970.

[8] T. A. McMahon, "The role of compliance in mammalian running gaits," *Journal of Experimental Biology*, vol. 115, no. 1, pp. 263–282, 1985.

[9] P. Nanua and K. J. Waldron, "Instability and chaos in quadruped gallop," *Journal of Mechanical Design*, vol. 116, no. 4, pp. 1096–1101, 1994.

[10] M. H. Raibert, "Running with symmetry," *The International Journal of Robotics Research*, vol. 5, no. 4, pp. 3–19, 1986.

[11] U. Culha and U. Saranli, "Quadrupedal bounding with an actuated spinal joint," in *Robotics and Automation (ICRA), 2011 IEEE International Conference on*, May 2011, pp. 1392–1397.

[12] B. Satzinger and K. Byl, "Control of planar bounding quadruped with passive flexible spine," in *International Symposium of Adaptive Motion in Animals and Machines*, March 2013, pp. 1392–1397.

[13] Q. Cao and I. Poulakakis, "Passive quadrupedal bounding with a segmented flexible torso," in *Intelligent Robots and Systems (IROS), 2012 IEEE/RSJ International Conference on*, Oct 2012, pp. 2484–2489.

[14] I. Poulakakis, E. Papadopoulos, and M. Buehler, "On the stability of the passive dynamics of quadrupedal running with a bounding gait," *The International Journal of Robotics Research*, vol. 25, no. 7, pp. 669–687, 2006.

[15] A. Sprowitz, A. Tuleu, M. Vespignani, M. Ajallooeian, E. Badri, and A. J. Ijspeert, "Towards dynamic trot gait locomotion: Design, control, and experiments with Cheetah-cub, a compliant quadruped robot," *The International Journal of Robotics Research*, 2013.

[16] G. C. Haynes, J. Pusey, R. Knopf, and D. E. Koditschek, "Dynamic bounding with a passive compliant spine," in *Proc. Dynamic Walking Conf*, 2012.

[17] D. Koepl and J. Hurst, "Force control for planar spring-mass running," in *Intelligent Robots and Systems (IROS), 2011 IEEE/RSJ International Conference on*, Sept 2011, pp. 129–130.

[18] A. Valenzuela and S. Kim, "Optimally scaled hip-force planning: A control approach for quadrupedal running," in *Robotics and Automation (ICRA), 2012 IEEE International Conference on*, May 2012, pp. 1901–1907.

[19] S. Eppinger and W. Seering, "Three dynamic problems in robot force control," in *Robotics and Automation (IRCRA), 1989 IEEE International Conference on*, May 1989, pp. 392–397 vol.1.

[20] L. D. Maes, M. Herbin, R. Hackert, V. L. Bels, and A. Abourachid, "Steady locomotion in dogs: temporal and associated spatial coordination patterns and the effect of speed," *Journal of Experimental Biology*, vol. 211, no. 1, pp. 138–149, 2008.

[21] M. H. Raibert, "Trotting, pacing and bounding by a quadruped robot," *Journal of Biomechanics*, vol. 23, Supplement 1, no. 0, pp. 79 – 98, 1990, international Society of Biomechanics.

[22] P. E. Hudson, S. A. Corr, and A. M. Wilson, "High speed galloping in the cheetah (acinonyx jubatus) and the racing greyhound (canis familiaris): spatio-temporal and kinetic characteristics," *Journal of Experimental Biology*, vol. 215, no. 1, pp. 2425–2434, 2012.

[23] T. S. Parker and L. O. Chua, *Practical numerical algorithms for chaotic systems*. Springer New York, 1989.

[24] J. Pratt, C.-M. Chew, A. Torres, P. Dilworth, and G. Pratt, "Virtual model control: An intuitive approach for bipedal locomotion," *The International Journal of Robotics Research*, vol. 20, no. 2, pp. 129–143, 2001.

[25] J. E. Pratt, "Exploiting inherent robustness and natural dynamics in the control of bipedal walking robots," Ph.D. dissertation, Massachusetts Institute of Technology, 2000.

[26] R. Murray, Z. Li, S. Sastry, and S. Sastry, *A Mathematical Introduction to Robotic Manipulation*. Taylor & Francis, 1994.